

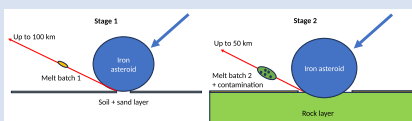
A two stage impact melting process in an impact glass strewn field from the Atacama Desert

P. Rochette^{1*}, G. Di Vincenzo², J. Gattacceca¹, J.A. Barrat³, B. Devouard¹,
L. Folco⁴, A. Musolino¹, Y. Quesnel¹



<https://doi.org/10.7185/geochemlet.2418>

Abstract



A new type of silica-rich glass has been discovered associated with the known impact glass strewn field of the Atacama Desert. Based on petrography, chemical composition and indistinguishable $^{40}\text{Ar}/^{39}\text{Ar}$ formation ages at *circa* 6.6 Ma, we infer that these two glasses were produced by the same impact event, which gave rise to two successive compositionally different melt batches in close succession. The first one is a silica-rich melt derived from a mixture of quartz sand and weathered magmatic rocks. It is reduced and devoid of extraterrestrial contamination. The second one, much more abundant and which corresponds to the normal glass, is oxidised, highly contaminated by the iron type impactor and derived from an underlying unweathered dacitic rock. This scheme sheds a new light on the first second of the interaction between the Earth surface and a large metallic asteroid.

rich melt derived from a mixture of quartz sand and weathered magmatic rocks. It is reduced and devoid of extraterrestrial contamination. The second one, much more abundant and which corresponds to the normal glass, is oxidised, highly contaminated by the iron type impactor and derived from an underlying unweathered dacitic rock. This scheme sheds a new light on the first second of the interaction between the Earth surface and a large metallic asteroid.

Received 16 December 2023 | Accepted 3 April 2024 | Published 3 May 2024

Introduction

Hypervelocity impacts on the Earth surface produce melts that can be ejected away from the crater (Glass and Simonson, 2013) at distance varying from 0.1 to less than 100 km for proximal ejecta or from 200 to 10,000 km for distal ejecta, such as tektites. Chemical and isotopic compositions of these melts may reflect provenance from the upper layers of the crust (Ma *et al.*, 2004; Rochette *et al.*, 2018), more or less contaminated by the extraterrestrial impactor (Koeberl, 2014), and showing variable compositions mimicking the heterogeneity of the target. Exploring the variabilities in the melt composition, target depth, and meteoritic contamination may help to understand details in the initial interactions between the impactor and the Earth surface. Such interactions have been already explored experimentally (Ebert *et al.*, 2014), in proximal ejecta around small craters (Hamann *et al.* 2018; Folco *et al.*, 2022), and in the largest ejecta known on Earth, the australasian tektite field (Folco *et al.*, 2023).

We recently described an impact glass strewn field extending over 50 km along a N120° azimuth in the Atacama Desert (Gattacceca *et al.*, 2021; Fig. 1). These black glasses, named atacamaites, are found as small splash-forms (average and maximum mass of 0.55 and 5.9 g, respectively), of dacitic composition. Their elemental and isotopic composition is compatible with an origin from local Andean magmatic rocks. The source crater has not been identified so far, but it was estimated to be relatively proximal (less than *circa* 100 km from the strewn field), based on the strong differences between atacamaites and *bona fide* tektites (see discussion in Gattacceca *et al.*, 2021). In particular

atacamaites show a relatively strong contamination by an iron meteorite impactor (likely IIAB type), on average 5 wt. % and up to 9 wt. %. They also contain a significant amount of magnetite, indicative of a large $\text{Fe}^{3+}/\text{Fe}_{\text{tot}}$ ratio. The fission track dating method was used to obtain a preliminary late Miocene age estimate.

A distal NW satellite of the main strewn field (Fig. 1) was briefly reported in Gattacceca *et al.* (2021). In that distinct area, extending away for over 50 km, rare small glass teardrops are found. Because of their distinctive light brown colour and translucent lustre, pointing toward a different bulk composition than the normal black and opaque atacamaites, one may challenge the hypothesis that they derive from the same impact. Studying this different glass type, hereafter named silica-rich glass, and comparing it to the normal atacamaites is the purpose of the present contribution. Methods used are described in Supplementary Information.

This glass strewn field is quite unique in the terrestrial record by being intermediate between proximal and distal glass ejecta, suggesting it may bring original clues on the impact melting and ejecta processes.

Results and Interpretation

Field work and petrography. In the satellite strewn field, we collected while searching for meteorites 25 translucent glass samples labelled EM in the El Medano dense collection area (DCA; Hutzler *et al.*, 2016), one sample in Caleta el Cobre DCA (labelled CEC) 25 km north of EM, and two samples 15 km southeast of

1. Aix-Marseille Université, CNRS, IRD, INRAE, CEREGE, Aix en Provence, France
2. Istituto di Geoscienze e Georisorse – CNR, via G. Moruzzi 1, 56124 Pisa, Italy
3. Univ Brest, CNRS, Ifremer, IRD, LEMAR, Plouzané, France
4. Dipartimento di Scienze della Terra, Università di Pisa, V. S. Maria 53, 56126, Pisa, Italy

* Corresponding author (email: rochette@cerge.fr)



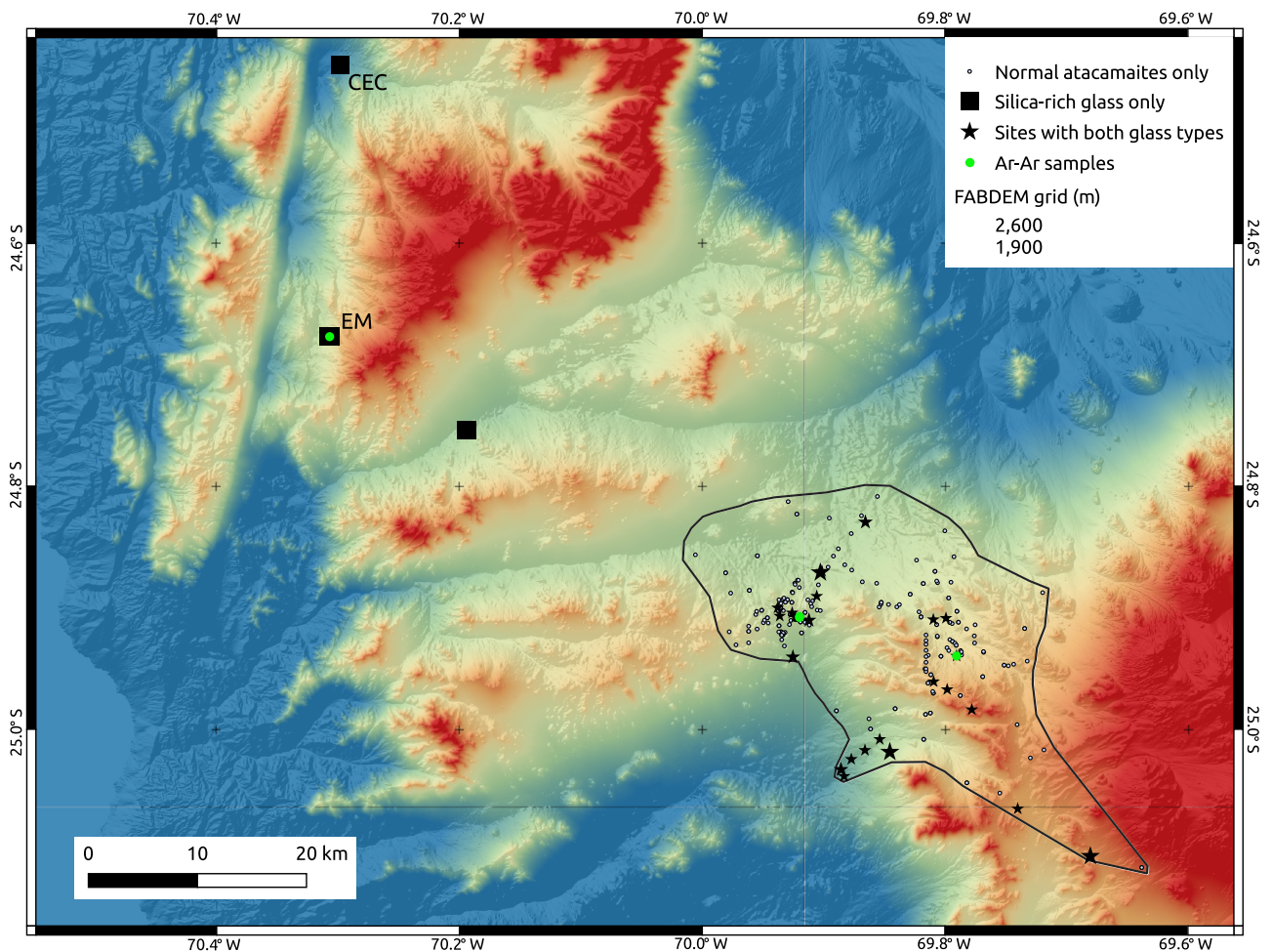


Figure 1 Map of the normal atacamaites strewn field, surrounded by a solid black line, together with locations of the silica-rich glass. Large stars correspond to sites with the largest proportion of silica-rich samples.

EM. Median and maximum sample masses are 0.16 and 0.78 g, respectively. Magnetic susceptibilities (χ) values range from 43 to $87 \times 10^{-9} \text{ m}^3/\text{kg}$. If one excludes the three samples with masses well below 90 mg this range reduces to $69\text{--}80 \times 10^{-9} \text{ m}^3/\text{kg}$, with a well-defined average of $76 \pm 3 \times 10^{-9} \text{ m}^3/\text{kg}$ ($n = 25$). Electron probe microanalysis (EPMA) on six samples give similar values of SiO_2 and $\text{Na}_2\text{O} + \text{K}_2\text{O}$ at 85.8 ± 0.7 and 0.32 ± 0.3 wt. %, respectively (Table S-1). Most samples have abraded teardrop shapes, but a few (the largest) are irregularly shaped with large bubbles (Fig. S-1). Optical and scanning electron microscopy of polished samples shows pervasive flow textures, vesicles and lechatelierite (*i.e.* pure silica glass) inclusions, often as twisted ribbons.

In the main strewn field systematic susceptibility measurements and an optical check of translucent character identified site K260 of Gattacceca *et al.* (2021) as rich in similar material: 53 samples, *i.e.* about 20 % of total samples of this site, have translucent character and $\chi < 85 \times 10^{-9} \text{ m}^3/\text{kg}$. The average χ of this population is $77 \pm 4 \times 10^{-9} \text{ m}^3/\text{kg}$. Twenty four other sampling sites from Gattacceca *et al.* (2021) possess one to four samples with the same features. Maximum and median masses of these silica-rich samples in the main strewn field are 2.3 and 0.21 g, respectively. In total, 99 silica-rich samples were identified in the main strewn field, *i.e.* about 1 % of the total collection. A map of the main strewn field (Fig. 1) indicates that the silica-rich glasses are scattered across most of the strewn field, with a slight tendency for more frequent occurrences in the southwestern part.

One translucent sample from site K260 exhibits a higher susceptibility ($169 \times 10^{-9} \text{ m}^3/\text{kg}$), an anomaly attributable to a 1 mm large black spherical inclusion. A polished section through this inclusion shows a glass spherule typical of normal atacamaites material (*i.e.* enriched in Fe and Ni), embedded into silica-rich glass (Fig. S-1, Table S-1). This supports the idea that both glasses were welded within a hot spray.

Magnetic susceptibility measurements of the silica-rich glasses show values in agreement with the lack of magnetite and a purely paramagnetic susceptibility due to Fe^{2+} only (see Rochette *et al.*, 2015; Fig. S-2). The corresponding reduced character of this glass is further confirmed by a consistently negative loss on ignition (average -0.25 wt. %; Table S-2).

$^{40}\text{Ar}/^{39}\text{Ar}$ dating. Three samples from the normal glass (samples K51, K48G, K326) and one (EM1a) from the silica-rich type were analysed by the $^{40}\text{Ar}/^{39}\text{Ar}$ dating method using both the laser step heating and the laser total fusion techniques. Details on the analytical procedure are given in the Supplementary Information. Uncertainties are given at 2σ . Accuracy was checked by analysing fragments of moldavite VLT2242 (Di Vincenzo, 2022). The full data set is listed in Table S-3.

Normal glass. All step heating experiments yielded reproducible flat or nearly flat age spectra, irrespective of the mass spectrometer utilised, with the exceptions of a few high temperature steps of data completed on samples K48G and K326 by the multi-collector noble gas mass spectrometer (Fig. S-3).

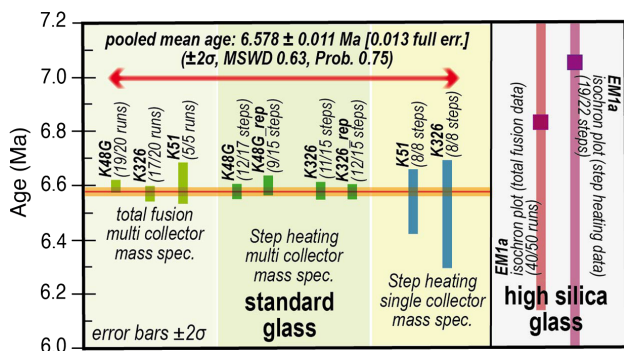


Figure 2 Summary of $^{40}\text{Ar}/^{39}\text{Ar}$ dates from step heating and total fusion data obtained in this study on normal glass (samples K48G, K326, K51) and a silica-rich glass (sample EM1a), through single and multi-collector mass spectrometers.

Concordant segments range from 65.3 to 100 % of the total $^{39}\text{Ar}_K$ released, with weighted mean dates indistinguishable within internal uncertainty, of 6.49 ± 0.20 to 6.60 ± 0.04 Ma (Fig. S-3). Data acquired using the multi-collector noble gas mass spectrometer yielded results with significantly lower analytical uncertainties and high temperature steps with apparent ages up to 6.7–7.0 Ma, suggestive of contamination by a minor extraneous Ar component (either excess or inherited Ar) heterogeneously distributed in the glass. Generally, total fusion data of single and a few glass fragments from the 0.35–0.50 mm grain fraction,

in agreement with step heating data, gave mostly within sample concordant dates, ranging from 6.565 ± 0.028 to 6.605 ± 0.072 Ma (Fig. S-3). Combining intra-sample concordant $^{40}\text{Ar}/^{39}\text{Ar}$ data from step heating and total fusion data yields a pooled mean age of 6.578 ± 0.011 Ma (± 0.013 including all known sources of errors; Fig. 2).

Silica-rich glass. Step heating data yielded statistically concordant age spectra for two aliquots of sample EM1a, although with some internal scatter, yielding indistinguishable apparent ages for the two aliquots of ~ 10 Ma (Fig. S-3). Analytical uncertainties are quite large when compared to $^{40}\text{Ar}/^{39}\text{Ar}$ data of the normal glass, because of the low gas yield due to the very low K contents of the high silica glass. Total fusion data of a few fragments of the same sample reveal instead a more complex picture, with single runs yielding apparent ages spanning over a large time interval of 7 to 14 Ma (Fig. S-3) most likely due an extraneous Ar component heterogeneously distributed in the glass. In an $^{36}\text{Ar}/^{40}\text{Ar}$ versus $^{39}\text{Ar}/^{40}\text{Ar}$ isochron diagram (Fig. S-4), both step heating and total fusion data define a triangular envelope which requires at least three distinct Ar components: (1) atmospheric Ar, (2) a radiogenic Ar component, located along the ordinate and yielding a date of ~ 6.5 –7 Ma, and (3) extraneous Ar with a $^{40}\text{Ar}/^{36}\text{Ar}$ ratio of ~ 320 . Selecting data points on the basis of their linearity and accepting linear regressions yielding a probability of fit $\geq 5\%$, the triangular envelope defined by step heating data is defined toward the $^{39}\text{Ar}/^{40}\text{Ar}$ x axis by nineteen data points (Fig. S-4) that define a linear array (MSWD = 1.43) with an apparent intercept age of 7.1 ± 1.4 Ma

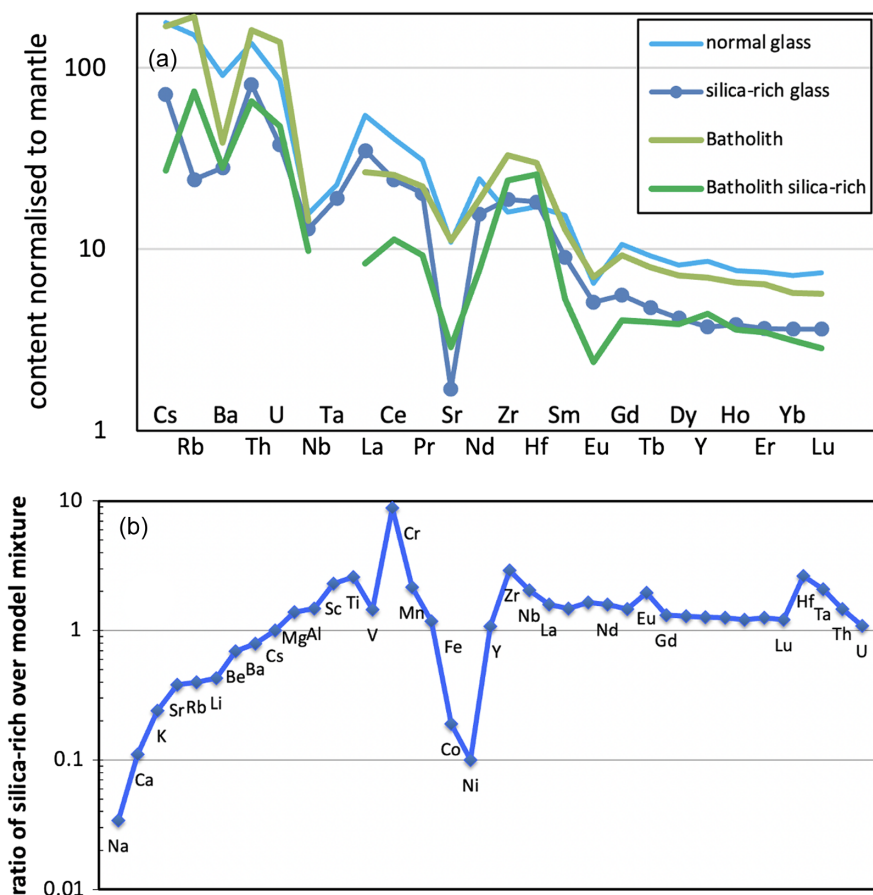


Figure 3 (a) Spidergram of trace elements normalised to primitive upper mantle (after McDonough and Sun, 1995) for the two glasses versus average coastal batholith data with SiO_2 content close to the glass and a compatible isotopic ratio (see Fig. S-5), (b) ratio of average composition of silica-rich glass to the average composition of normal glass corrected from quartz addition. Alkali elements appear first, ordered by increasing ratio, then the other elements with increasing atomic weight.



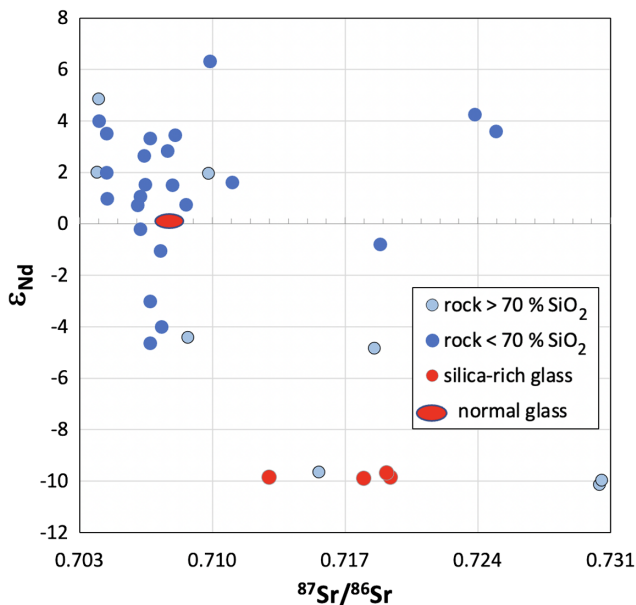


Figure 4 ϵ_{Nd} versus $^{87}\text{Sr}/^{86}\text{Sr}$ for normal atacamaite glass (red ellipse after Gattacceca *et al.*, 2021), silica-rich glass (red dots) and magmatic rocks from a two degree square centred on the main strewn-field (24–26° S, 66.5–68.5° W), extracted from Oliveros *et al.* (2020) database, cut above $\text{SiO}_2 = 60$ wt. %. Dark and light blue corresponds to rock with less or more than 70 wt. % SiO_2 .

and a $^{40}\text{Ar}/^{36}\text{Ar}$ y intercept of 316.5 ± 9.4 . Likewise, the triangular envelope defined by total fusion data is defined toward the $^{39}\text{Ar}/^{40}\text{Ar}$ x axis by forty data points (Fig. S-4) that define a linear array (MSWD = 1.20) with an apparent intercept age of 6.83 ± 0.69 Ma and a $^{40}\text{Ar}/^{36}\text{Ar}$ y intercept of 321.9 ± 4 . The pooled mean age from the high silica glass of 6.87 ± 0.62 Ma, suggests an indistinguishable age for the two glass types within 0.29 ± 0.62 Ma ($\pm 2\sigma$; Fig. 2).

Geochemistry. For detailed geochemical analysis, three silica-rich samples were selected from the western satellite strewn field (Fig. 1) and three others from different sites in the main strewn field. The six silica-rich samples are characterised by an average SiO_2 content of 85.4 ± 0.3 wt. % compared to 63.7 ± 2.9 wt. % for normal atacamaites (Table S-2). Variability (max/min –1) is below 20 % for the majority of elements including Si, Al, Fe, K, Ti, rare earths and a number of other trace elements. This points toward a rather homogeneous melt batch, including the main strewn field samples. No significant difference is observed between samples from the satellite strewn field, and silica-rich samples from the main strewn field. A trace element spidergram (Fig. 3a, Table S-4) indicates that normal atacamaites have patterns typical of the mainly dacitic local Jurassic batholith (compared to Lucassen *et al.*, 2006; Oliveros *et al.*, 2020). On the other hand, the silica-rich glass has significant depletion in Cs, Rb, Sr that cannot be accounted for by a more differentiated magma, but points toward a weathering effect. The total alkali content of 0.35 ± 0.01 wt. % is also consistent with strong weathering (Fig. S-5). We tested the hypothesis that the high silica glass derived from a mixture of 40.2 wt. % normal atacamaite and 59.8 wt. % quartz sand present as a layer covering the dacitic magmatic target (proportion matched to give equal SiO_2 content). The ratio of the real silica-rich glass to the modelled normal atacamaite + quartz mixture is shown in Figure 3b. A strong deficit of alkali elements, especially for the lighter ones, is evidenced, as well as a deficit of Co and Ni. We may thus propose that alkali depletion is due to the dissolution of feldspars while Co and Ni depletion is due to

negligible extraterrestrial contamination in the silica-rich glass compared to the normal glass (see discussion in Supplementary Information). Regarding the other enriched elements, those enriched by a factor of more than 2 are Sc, Ti, Cr, Mn, Zr, Nb, Hf, Ta. This may be explained by addition of sand heavy minerals such as chromite and zircon. To summarise, the silica-rich glass could be derived by melting a weathered dacitic target of similar composition as normal atacamaite, together with quartz sand and heavy minerals.

This interpretation can be confronted with the isotopic compositions of Sr and Nd (Fig. 4, Table S-5). With an $^{87}\text{Sr}/^{86}\text{Sr}$ value of 0.713 for K260 sample and an average of 0.719 for the three samples from the satellite strewn field, the silica-rich glass is more radiogenic than the normal glass that has an $^{87}\text{Sr}/^{86}\text{Sr}$ ratio < 0.708 . Most local rocks have $^{87}\text{Sr}/^{86}\text{Sr}$ below 0.710, and the ones with ratios higher than 0.718 are silica-rich. The Nd isotopic ratio also shows a distinct signature for the two glasses. The isotopic data thus invalidate the simple model based on element data alone, and indicate that the magmatic component in the silica-rich glass does not have the same isotopic signature as the source of normal atacamaite.

Discussion and Conclusions

Based on indistinguishable formation ages within uncertainties, on the geochemical constraints, on the observation that both normal glass and high silica glass coexist within a single sample and the fact that chemically identical silica-rich glasses are present in both the main and the satellite strewn fields, a single impact event seems to be the most likely hypothesis. In addition, the alternative hypothesis that the two glass types were generated by two independent impacts seems to be an unlikely possibility based on a probabilistic basis. Indeed, following the model proposed by Rochette *et al.* (2023), one can compute the probability that a second impact occurred within a maximum 0.9 Ma time window (based on the uncertainties of $^{40}\text{Ar}/^{39}\text{Ar}$ ages) and within 100 km distance from the one producing the normal atacamaites. This probability is 0.4 % for a crater > 1 km diameter.

Therefore, we can put forward a scenario of impact melting of the Atacama Desert surface in two stages (Fig. S-6). In the first stage, the upper metres of the target, consisting of aeolian sands and weathered regolith derived from magmatic materials (*e.g.*, tephra or transported detritus), is melted and reduced without significant impactor contamination, and ejected toward both the western satellite and the main strewn fields. Fractions of a second later an underlying unweathered dacitic rock is melted in greater quantity, mixed variably with the oxidised sprayed impactor, and ejected only in the main strewn field, *i.e.* over a shorter distance than the first batch (about 50 km less). Surface regolith cannot simply derive from the underlying dacite as isotopic data and trace element patterns do not match, but it may derive from a mixture of late tephra and/or degradation of transported local rocks. Another type of scenario is a lateral chemical and/or lithological contrast within the melted surface, *e.g.*, made of a fresh dacitic outcrop surrounded by a regolith, with synchronous melting. However, we favour the vertical layering scenario based on the principle of Occam's razor and the fact that the lateral contrast scenario does not provide a logical sequential scenario for the impactor contamination contrast. In our scenario the first melt, heated by radiating compressed air, is not interacting with the impactor spray. This scenario, compatible with theoretical impact modelling (Artemieva, 2002; Wakita *et al.*, 2022; Carlson *et al.*, 2023), also implies that the first melt batch was ejected farther than the more abundant second one. As a consequence, it is expected that the source

crater should be located closer to the main strewn field. The source crater is tentatively located along the apparent ejecta lobe oriented N120°, East of the main strewn field (Fig. 1).

Geochemically distinct types of ballistically ejected impact glasses linked to a single impact event have been described in the literature, such as around the Zhamanshin and Kamil craters (Jonasova *et al.*, 2016; Fazio *et al.*, 2016). However, the 100 km wide atacamaite strewn field is a rather unique example where the kinematics of impactor-target interaction can be traced with such detail. The second largest comparable case, the Darwin 50 km wide strewn field, does show chemical variability but not with such a dichotomy in particular in impactor contamination and redox state (Howard, 2008). The origin of the reduction observed in the silica-rich glass remains a puzzle: one could invoke biomass carbon, as advocated for the fire derived Pica glass in northern Atacama (Roperch *et al.*, 2017) and the Darwin glass (Howard *et al.*, 2013). The Libyan Desert glass strewn field is larger than the atacamaite one, but its extension is suspected to be related to fluvial transport (Jimenez-Martinez *et al.*, 2015) and it shows no evidence of ballistic transport. It is therefore not a relevant comparison.

Acknowledgements

The Ar laser probe facility was realised with the financial support of CNR. We acknowledge R. Romero, who provided eight more Si-rich samples, as well as the input of one anonymous reviewer, K. Howard and Journal editor that helped improving our manuscript. Work partly supported by the ANR ET-Megafire project (ANR-21-CE49-0014-03).

Editor: Romain Tartèse

Additional Information

Supplementary Information accompanies this letter at <https://www.geochemicalperspectivesletters.org/article2418>.



© 2024 The Authors. This work is distributed under the Creative Commons Attribution Non-Commercial No-Derivatives 4.0

License, which permits unrestricted distribution provided the original author and source are credited. The material may not be adapted (remixed, transformed or built upon) or used for commercial purposes without written permission from the author. Additional information is available at <https://www.geochemicalperspectivesletters.org/copyright-and-permissions>.

Cite this letter as: Rochette, P., Di Vincenzo, G., Gattacceca, J., Barrat, J.A., Devouard, B., Folco, L., Musolino, A., Quesnel, Y. (2024) A two stage impact melting process in an impact glass strewn field from the Atacama Desert. *Geochem. Persp. Let.* 30, 28–33. <https://doi.org/10.7185/geochemlet.2418>

References

- ARTEMIEVA, N. (2002) Tektite origin in oblique impact: numerical modelling. In: KOEBERL, C. PLADO, J. (Eds.) *Impacts in Precambrian Shields*, Springer-Verlag, Berlin, 257–276. https://doi.org/10.1007/978-3-662-05010-1_10
- CARLSON, M.A., MELOSH, H.J., JOHNSON, B.C. (2023) Atmospheric Interactions of Ejecta on Earth and Mars Including the Effect of Vaporization. *The Planetary Science Journal* 4, 194. <https://doi.org/10.3847/PSJ/ac9f1>
- DI VINCENZO, G. (2022) High precision multi-collector $^{40}\text{Ar}/^{39}\text{Ar}$ dating of moldavites (Central European tektites) reconciles geochronological and paleomagnetic data. *Chemical Geology* 608, 121026. <https://doi.org/10.1016/j.chemgeo.2022.121026>
- EBERT, M., HECHT, L., DEUTSCH, A., KENKMANN, T., WIRTH, R., BERNDT, J. (2014) Geochemical processes between steel projectiles and silica-rich targets in hypervelocity impact experiments. *Geochimica et Cosmochimica Acta* 135, 257–279. <https://doi.org/10.1016/j.gca.2014.02.034>
- FAZIO, A., D'ORAZIO, M., CORDIER, C., FOLCO, L. (2016) Target-projectile interaction during impact melting at Kamil Crater, Egypt. *Geochimica et Cosmochimica Acta* 18, 33–50. <http://dx.doi.org/10.1016/j.gca.2016.02.003>
- FOLCO, L., CARONE, L., D'ORAZIO, M., CORDIER, C., SUTTLE, M.D., VAN GINNEKEN, M., MASOTTA, M. (2022) Microscopic impactor debris at Kamil Crater (Egypt): The origin of the Fe-Ni oxide spherules. *Geochimica et Cosmochimica Acta* 335, 297–322. <https://doi.org/10.1016/j.gca.2022.06.035>
- FOLCO, L., ROCHETTE, P., D'ORAZIO, M., MASOTTA, M. (2023) The chondritic impactor origin of the Ni-rich component in Australasian tektites and microtektites. *Geochimica et Cosmochimica Acta* 360, 231–240. <https://doi.org/10.1016/j.gca.2023.09.018>
- GATTACCECA, J., DEVOUARD, B., BARRAT, J.A., ROCHETTE, P., BALESTRIERI, M.L., BIGAZZI, G., MÉNARD, G., MOUSTARD, F., DOS SANTOS, E., SCORZELLI, R., VALENZUELA, M. (2021) A 650 km² Miocene strewn field of splash-form impact glasses in the Atacama Desert, Chile. *Earth and Planetary Science Letters* 569, 117049. <https://doi.org/10.1016/j.epsl.2021.117049>
- GLASS, B.P., SIMONSON, B.M. (2013) *Distal Impact Ejecta Layers: A Record of Large Impacts in Sedimentary Deposits*. Springer, Heidelberg. <https://doi.org/10.1007/978-3-540-88262-6>
- HAMANN, C., FAZIO, A., EBERT, M., HECHT, L., WIRTH, R., FOLCO, L., DEUTSCH, A., REIMOLD, W.U. (2018) Silicate liquid immiscibility in impact melts. *Meteoritics and Planetary Science* 53, 1594–1632. <https://doi.org/10.1111/maps.12907>
- HOWARD, K.T. (2008) Geochemistry of Darwin glass and target rocks from Darwin crater, Tasmania, Australia. *Meteoritics and Planetary Science* 43, 479–496. <https://doi.org/10.1111/j.1945-5100.2008.tb00667.x>
- HOWARD, K.T., BAILEY, M.J., BERHANU, D., BLAND, P.A., CRESSEY, G., HOWARD, L.E., JEYNES, C., MATTHEWMAN, R., MARTINS, Z., SEPHTON, M.A., STOJANOV, V., VERCHOVSKY, S. (2013) Biomass preservation in impact melt ejecta. *Nature Geoscience* 6, 1018–1022. <https://doi.org/10.1038/ngeo1996>
- HUTZLER, A., GATTACCECA, J., ROCHETTE, P., BRAUCHER, R., CARRO, B., CHRISTENSEN, E.J., COURNEDE, C., GOUNELLE, M., LARIDHI OUAZAA, N., MARTINEZ, R., VALENZUELA, M., WARNER, M., BOURLES, D. (2016) Description of a very dense meteorite collection area in western Atacama: Insight into the long-term composition of the meteorite flux to Earth. *Meteoritics and Planetary Science* 51, 468–482. <https://doi.org/10.1111/maps.12607>
- JIMENEZ-MARTINEZ, N., RAMIREZ, M., DIAZ-HERNANDEZ, R., RODRIGUEZ-GOMEZ, G. (2015) Fluvial Transport Model from Spatial Distribution Analysis of Libyan Desert Glass Mass on the Great Sand Sea (Southwest Egypt): Clues to Primary Glass Distribution. *Geosciences* 5, 95–116. <https://doi.org/10.3390/geosciences5020095>
- JONÁŠOVÁ, Š., ACKERMAN, L., ŽÁK, K., SKÁLA, R., ĎURIŠOVÁ, J., DEUTSCH, A., MAGNA, T. (2016) Geochemistry of impact glasses and target rocks from the Zhamanshin impact structure. *Geochimica et Cosmochimica Acta* 190, 239–264. <https://doi.org/10.1016/j.gca.2016.06.031>
- KOEBERL, C. (2014) 2.5 - The Geochemistry and Cosmochemistry of Impacts. In: HOLLAND, H.D., TÜREKIAN, K.K. (Eds.) *Treatise on Geochemistry*. Second Edition, Elsevier, Amsterdam, 73–118. <https://doi.org/10.1016/B978-0-08-095975-7.00130-3>
- LUCASSEN, F., KRAMER, W., BARTSCH, V., WILKE, H.-G., FRANZ, G., ROMER, R.L., DULSKI, P. (2006) Nd, Pb, and Sr isotope composition of juvenile magmatism in the Mesozoic large magmatic province of northern Chile (18–27°S): indications for a uniform subarc mantle. *Contributions to Mineralogy and Petrology* 152, 571–589. <https://doi.org/10.1007/s00410-006-0119-y>
- MA, P., AGGREGY, K., TONZOLA, C., SCHNABEL, C., DE NICOLA, P., HERZOG, G.F., WASSON, J.T., GLASS, B.P., BROWN, L., TERA, F., MIDDLETON, R. (2004) Beryllium-10 in Australasian tektites: constraints on the location of the source crater. *Geochimica et Cosmochimica Acta* 68, 3883–3896. <https://doi.org/10.1016/j.gca.2004.03.026>
- MCDONOUGH, W.F., SUN, S.-S. (1995) The composition of the Earth. *Chemical Geology* 120, 223–253. [https://doi.org/10.1016/0009-2541\(94\)00140-4](https://doi.org/10.1016/0009-2541(94)00140-4)
- OLIVEROS, V., MORENO-YAEGER, P., FLORES, L. (2020) Igneous Rock Associations 25. Pre-Pliocene Andean Magmatism in Chile. *Geoscience Canada* 47, 65–82. <https://doi.org/10.12789/geocanj.2020.47.158>
- ROCHETTE, P., GATTACCECA, J., DEVOUARD, B., MOUSTARD, F., BEZAEVA, N.S., COURNEDE, C., SCAILLET, B. (2015) Magnetic properties of tektites and other related impact glasses. *Earth and Planetary Science Letters* 432, 381–390. <https://doi.org/10.1016/j.epsl.2015.10.030>
- ROCHETTE, P., BRAUCHER, R., FOLCO, L., HÖRNG, C.S., AUMAÎTRE, G., BOURLÈS, D.L., KEDDADOUCHE, K. (2018) ^{10}Be in Australasian microtektites compared to



- tektites: Size and geographic controls. *Geology* 46, 803–806. <https://doi.org/10.1130/G45038.1>
- ROCHETTE, P., BARATOUX, D., BRAUCHER, R., CORNEC, J., DEBAILLE, V., DEVOUARD, B., GATTACCECA, J., GOUNELLE, M., JOURDAN, F., MOUSTARD, F., NOMADE, S. (2023) Linking a distal ejecta with its source crater: a probabilistic approach applied to tektites. *Comptes Rendus Geosciences* 355, 145–155. <https://doi.org/10.5802/crgeos.206>.
- ROPERCH, P., GATTACCECA, J., VALENZUELA, M., DEVOUARD, B., LORAND, J.P., ARRIAGADA, C., ROCHETTE, P., LATORRE, C., BECK, P. (2017) Surface vitrification caused by natural fires in Late Pleistocene wetlands of the Atacama Desert. *Earth and Planetary Science Letters* 469, 15–26. <https://doi.org/10.1016/j.epsl.2017.04.009>
- WAKITA, S., GENDA, H., KUROSAWA, K., DAVISON, T.M., JOHNSON, B.C. (2022) Effect of impact velocity and angle on deformational heating and postimpact temperature. *Journal of Geophysical Research: Planets* 127, e2022JE007266. <https://doi.org/10.1029/2022JE007266>